Tectonophysics 664 (2015) 191–201

Contents lists available at ScienceDirect

Tectonophysics

journal homepage: www.elsevier.com/locate/tecto

Holocene shortening rates of an Andean-front thrust, Southern Precordillera, Argentina

Carlos H. Costa [a,*], Emilio A. Ahumada [a], Fabricio R. Vázquez [a,b], Daniela M. Kröhling [b,c]

[a] Departamento de Geología, Universidad Nacional de San Luis, Ejército de los Andes 950, Bloque II, 5700 San Luis, Argentina
[b] CONICET, Buenos Aires, Argentina
[c] Universidad Nacional del Litoral, CC 217, 3000 Santa Fe, Argentina

ARTICLE INFO

Article history:
Received 18 May 2015
Received in revised form 16 September 2015
Accepted 18 September 2015
Available online 30 September 2015

Keywords:
Andean thrusts
Orogenic front
Shortening rates
Neotectonics
Holocene
Argentine Precordillera

ABSTRACT

A significant part of the Quaternary shortening between the Chilean trench and the relative stable interior of the South American plate at the Pampean flat slab (27–33°S), has been accommodated at the eastern foothills of the Andes and mainly within a narrow neotectonic belt along the eastern side of the Argentine Precordillera. Tectonic geodesy results point out that this area is being shortened at a ~2–4 mm/a rate, whereas shortening rates estimated over longer time periods (1–20 Ma) suggest values ranging from 1 mm/a to 16 mm/a. Geomorphic and geologic evidence indicate that the east-directed Las Higueras Thrust System is one of the main structures that has accommodated Quaternary deformation at this section of the Andean orogenic front (32° 05′–32° 35′S). An outcrop exhibiting the thrust propagation into fluvial sediments allows the Holocene shortening rates at the northern end of this structure to be estimated, based on retrodeformation of Holocene strata and radiocarbon dating of two charcoal-bearing beds. Estimated shortening rates yielded mean values of 1.90 ± 0.28 mm/a for the last 4495 ± 143 cal yr BP and 1.53 ± 0.26 for the last 8245 ± 48 cal yr BP. These results pose some uncertainties due to the incompleteness of the exposed deformation at the hanging wall. However, they correspond to a key timescale which helps to bridge the gap between rates derived from the short-term GPS data and the long-term permanent deformation rates obtained through geologic studies. Although the estimated rates suggest that slip on the thrust could have accelerated during the last ~4 ka, more data are necessary to reliably address this key issue.

1. Introduction

Active orogenic processes at the Southern Pampean flat-slab segment of the Central Andes in Argentina (31°–33°S) have been concentrated since the Pliocene along the eastern piedmont of the Precordillera (Fig. 1) (Jordan et al., 1983; Ramos, 1988; Ramos et al., 2002). Tectonic geodesy has illuminated the present kinematic framework for the last two decades (Brooks et al., 2003; Kendrick et al., 1999, 2001, 2003, 2006), indicating that changes in the crustal velocity field at these latitudes are concentrated between the Precordillera fold and thrust belt and the Sierras Pampeanas broken-foreland region at estimated rates of ~2–4 mm/a (Brooks et al., 2003; Kendrick et al., 2006) (Fig. 1). This fact is also underlined by the concentration of Quaternary-active contractional structures (Bastías et al., 1984; Cortés et al., 1999; Costa et al., 2000a, 2006a, 2014; Meigs et al., 2006; Siame et al.,, 2002, 2005, 2006; Vergés et al., 2007; Rockwell et al., 2014; Schmidt et al., 2011, and many others) and by the most significant crustal seismicity in Argentina (Smalley and Isacks, 1987, 1990; INPRES, 1989; Smalley et al., 1993; Alvarado et al., 2007). Several destructive crustal earthquakes (M > 7.0) have been located since the nineteenth century within this region, such as those which seriously damaged the urban areas of Mendoza city in 1861 and San Juan city in 1944 and 1977 (Fig. 1).

However, to recognize how long-, intermediate-, and short-term rates compare to one another and how upper crustal deformation is accommodated through individual structures, remains a core issue for a better understanding of the Andean building processes. In fact, some contributions have discussed the consistency between geologic and geodetic data and their implications for the current knowledge of the Andean orogeny (e.g. Hindle et al., 2002; Salomon et al., 2013; Schmidt et al., 2011; Siame et al., 2002).

There is a time gap in the existing data on the Andean deformation between the short-term rates derived from GPS measurement and the long-term rates provided by geologic data dominated by anelastic permanent deformation (10^6–10^7 years) (See Table 1). Neotectonic and paleoseismic studies can help in the completion of the dynamic record of individual structures during millennial time scales and therefore can contribute to provide data in a time span not well covered by the techniques and studies mentioned above.

An arid climate and suitable morphotectonic conditions have turned the Andean orogenic front along the 60 km-long Las Peñas-Las Higueras

* Corresponding author.
E-mail address: costa@unsl.edu.ar (C.H. Costa).

http://dx.doi.org/10.1016/j.tecto.2015.09.017
0040-1951/

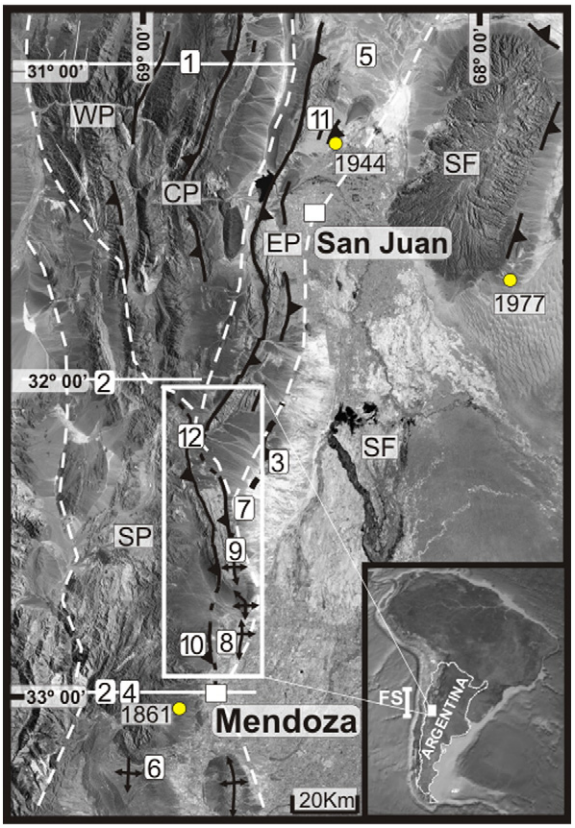

Fig. 1. Main tectonic settings in the Precordillera in central western Argentina between 31°S and 33°S, showing the major neotectonic faults and folds in black trace. The white rectangle corresponds to the area of the Las Peñas–Las Higueras range (see Fig. 2). White dashed lines correspond to internal boundaries in the Precordillera. WP, Western Precordillera; CP, Central Precordillera; EP, Eastern Precordillera; SP, Southern Precordillera; SF, Sierras Pampeanas and foreland plains; FS: Flat slab subduction segment (in inset). Structures in the north of the Eastern Precordillera correspond to the Villicum-Las Tapias and La Laja thrusts. Yellow circles indicate the epicenter location for the most significant damaging historic earthquakes mentioned in the text. Numbers in white boxes refer to studies on shortening rates compiled in Table 1.

range into one of the best exposures of active thrust faulting along the entire Andes (Figs. 1 and 2). An exposure of the Las Higueras thrust (LHT) at the Montaña river (Figs. 2, 3, 4 and 5), along with charcoal-bearing beds suitable for ^{14}C dating, have allowed to estimate the shortening rate for this structure during the last ~ 8 ka. These results provide new data for complementing the time coverage among rates derived from different approaches and time windows. This contribution also aims to compare the rates here proposed with other results already reported at different locations along the Andean thrust front between 31–33°S. Table 1 illustrates shortening rates reported along this region, encompassing different time scales for individual structures or regions and obtained through different techniques.

2. Tectonic setting

The eastern margin of the Argentine Precordillera has been the locus of the Andean building processes since the Pliocene, concentrating the most significant Quaternary deformation in the country (Bastías et al., 1984, 1993;; Cortés et al., 1999; Costa et al., 2000a, 2006a, 2006b, 2014; Siame et al., 2002, 2005, 2006; Perucca and Paredes, 2002; Schmidt et al., 2011; Salomon et al., 2013; Perucca and Vargas, 2014, among others) (Fig. 1). This nN-S-trending fold and thrust-belt exhibits different neotectonic styles at the frontal deformation zone. North of 32°10′S the orogenic front is emplaced at the Eastern Precordillera (EP in Fig. 1), characterized by west-directed (Pampean-type) thrusts cored by the Sierras Pampeanas basement (Ortiz and Zambrano, 1981; Perucca and Ruiz, 2014; Zapata and Allmendinger, 1996). These Pampean-type thrusts have also been understood as being the result of crustal wedging (Meigs and Nabelek, 2010; Meigs et al., 2006; Vergés et al., 2007). The most conspicuous evidence of Quaternary deformation is here represented by back limb-tightening structures at its eastern hillslope, linked to reverse faults with variable dip angles and related rectilinear scarps (Costa et al., 1999, 2006a; Meigs et al., 2006; Ragona, 2007; Rockwell et al., 2014; Vergés et al., 2007).

Quaternary deformation along the Andean front south of 32°10′S lies mostly at the Southern Precordillera domain (SP in Fig. 1), which is characterized by NNW-SSE striking east-directed (Andean-type) thrusts, controlled by the geometry of an inverted Mesozoic rift basin (Cortés et al., 2005, 2014; Dellapé and Hegedus, 1995; Ramos and Kay, 1991). The transfer area located between the opposite-verging thrusts of the Eastern and Southern Precordillera, corresponds to a triangle zone with an antithetic-linkage array (Ahumada, 2010; Ahumada and Costa, 2009; Figueroa and Ferraris, 1989; Vergés et al., 2007).

The main morphostructure along the orogenic front exposed at the Southern Precordillera corresponds to the Las Peñas-Las Higueras range. Quaternary activity is here concentrated along the west-dipping Las Higueras and the Las Peñas thrusts (Figs. 1 and 2) (Ahumada and Costa, 2009; Cortés and Costa, 1996; Costa et al, 2000a, 2005, 2014; Harrington, 1971; Schmidt et al., 2011). The Las Peñas thrust is the eastern bounding-fault of the range, placing Neogene sedimentary rocks over thick Quaternary alluvial deposits along ~43 km with moderate to low dipping angles. Its geometry and Quaternary activity has been described at several places along its trace, as well as the structural features characterizing their northern and southern ends (Ahumada, 2010; Ahumada and Costa, 2009; Cortés and Costa, 1996; Costa et al., 2000a, 2005, 2014; Schmidt et al., 2011). Primary tectonic landforms are not always present, but when preserved they are characterized by east-facing fold-limb scarps deforming river terrace levels of different ages (Ahumada and Costa, 2009; Costa et al., 2000a, 2005, 2014; Schmidt et al., 2011). Quaternary activity along the Las Higueras thrust has been reported by Ahumada (2004); Ahumada et al. (2006); Ahumada and Costa (2009) and Ahumada (2010).

3. The Las Higueras thrust (LHT)

The LHT extends 90 km with a general NNW-SSE orientation (Figs. 1 and 2). Its trace is delineated by a significant slope-break along most parts of the Las Peñas-Las Higueras range, and cuts through Paleozoic-Mesozoic sedimentary and volcanic rocks over Mesozoic-Cenozoic sedimentary sequences (Wichmann, 1928; Dessanti, 1942; Fossa Mancini, 1942; Harrington, 1971; Figueroa and Ferraris, 1989; Costa et al., 2000a; Ahumada et al., 2006, among others). It can be subdivided into three sections with different morphotectonic characteristics (Fig. 2). The northern section (A in Fig. 2) (32°05′–32°20′S) constitutes the main mountain-piedmont junction at the northern part of the Las Peñas-Las Higueras range, as well as the west-bounding structure of the linkage zone between the Southern and Eastern Precordillera (Ahumada, 2010; Ahumada and Costa, 2009) (Fig. 1). The thrust surface dips 30°W–45°W with a general NNW-SSE trend and exhibits several bends in plan view (Fig. 2). This section show evidences of Quaternary activity such as fold-limb scarps and faulted bajadas deposits. Its northernmost part behaves as a blind thrust propagating into alluvial deposits, as reported between 32°14′S and the latitude of the outcrop here examined (Ahumada and Costa, 2009; Ahumada, 2010) (Fig. 3). The central thrust section (B in Fig. 2) (32°20′–32°34′S) includes the highest range elevations, characterized by the outcrops of resistant Triassic sedimentary rocks and early Paleozoic limestones (San Juan Formation). The recognition of diagnostic neotectonic evidence along its length is hampered by elusive exposures and a coarse colluvial-fluvial cover overlying the thrust trace. Descriptions of the thrust surface refer to an east-dipping fault zone ranging between 45°E and 80°E (Ahumada, 2004), emplacing the referred lithologies over

Table 1
Summary of shortening rate estimation for the Southern Pampean flat-slab segment, involving different time scales. Values refer to shortening rates, unless specified. (U) uplift rate. See Fig. 1 for location.

Reference	Location (see Fig. 1)	Region/structure	Time window	Rate
Million year time scale				
Allmendinger et al. (1990) Jordan et al. (1993)	1	Central/Western Precordillera (30–31°S) (1)	20 Ma	6.3–9.5 mm/a
Ramos et al. (1996)		Principal Cordillera (Aconcagua FTB) (30°50′ S)	<20 Ma	4.7–6.0 mm/a
Cristallini and Ramos (1997)	2	Precordillera, Frontal &Principal Cordilleras (32–33°S) (2)	<20 Ma 20–9.2 Ma	5 mm/a 2.2 mm/a
Ramos et al. (2004)	2	Precordillera & Principal/Frontal Cordilleras (32–33°S) (2)	20 Ma	5.5–7.7 mm/a
Vergés et al. (2007)	3	Cerro Salinas thrust (32°10′S) (3)	8.5 Ma	1 mm/a
Giambiagi and Ramos (2002)	4	Southern Precordillera (33°S) (4)	~7 Ma	~4,3 mm/a
Ramos et al. (2002)		Eastern Precordillera & Bermejo Basin (30°30′S)	3 Ma	6.5 mm/a
Zapata and Allmendinger (1996)	5	Eastern Precordillera (30–31°S) (5)	~2 Ma	5.5 mm/a
Sarewitz (1988)	6	Piedmont anticlines – La Pilona (33°S) (6)	2.7–1.0 Ma	6 (16) mm/a
Costa et al.(2000b)	7	Montecito Anticline (32°25′S) (7)	1–3 Ma	>0.04–0.15 mm/a (U)
Millennial time scale				
Cisneros et al. (2010) Schoenbohm et al. (2013)	3	Cerro Salinas thrust (32°10′S) (3)	Late Pleistocene	>0.13 mm/ a (U)
Olgiati and Ramos (2003)	8	Capdevila & Borbollón anticlines (32°45′S) (8)	~20 ka	0.1–0.3 mm/a
Schmidt et al. (2011)	9	Las Peñas thrust (32°31′S) (9)	12 ka	1.2–2.0 mm/a
Schmidt et al. (2011)	10	Cerro La Cal fault (32°42′S) (10)	12 ka	~1 mm/a
Salomon et al.(2013)		Cerro La Cal fault (32°42′S)	3.9 ka 0.8 ka 770 ± 150 a	1.5 ± 0.3 mm/a 5.2 ± 1.5 – 5.3 ± 1.3 mm/a.
Rockwell et al.(2014)	11	La Laja fault (11)	35 ka	~0.8 mm/a
Bohon et al. (2008)	7	Montecito Anticline (32°25′S) (7)	7 ka	~0.65 mm/a (U)
This contribution	12	Las Higueras Thrust System (32°07′S) (12)	~8 ka	1.27–2.18 mm/a
Decadal time scale				
Kendrick et al. (1999: 2001; 2003)		Andean Front (20–36°S)		2–7 mm/a
Brooks et al. (2003)		Andean Front (32–33°S)		4.5 ± 1.7 mm/a
Kendrick et al. (2006)		Southern Precordillera (32–33°S)		~3–4 mm/a

Mesozoic and Cenozoic continental deposits. Although Quaternary beds have not been observed affected by the thrust propagation, Quaternary tectonic activity at the central section cannot be ruled out (Ahumada, 2004). At the Las Peñas river (Fig. 2), the related shear zone involves limestone, sandstone and conglomerates of the hanging wall sequence. It corresponds to an upthrust and locally overturned fault surface (85°E) (Bea, 2000). The high dip angle might be attributed to the bedding geometry and to cumulated tilting related to the eastward propagation of the Quaternary deformation front.

The southern section of the LHT (C in Fig. 2) (32°34′–32°53′S?) comprises the southernmost low hills and the surrounding piedmont, with almost no pre-Quaternary substratum cropping-out at the hanging-wall, except for the La Bomba and the Cerro La Cal hills (Fig. 2). East-facing scarps outlining the thrust trace vanish below the urban area of Mendoza city. Mingorance (2006) claimed that this fault section corresponds to the source for the M 7.0 1861 Mendoza earthquake, interpreting primary coseismic ruptures along it during such event. The rupture surface in Late Pleistocene-Holocene sediments also exhibits a west-dipping angle ranging between 16° to 38° (Mingorance, 2006) and evidences of activity during the last ca. 800 years (Schmidt et al., 2012). Previous studies have considered the Cerro La Cal fault as the southern edge of the LHT (Figueroa and Ferraris, 1989; Bastías et al., 1993; Ahumada, 2004; Ahumada et al., 2006, among others). It is difficult to assure the physical continuity of the Las Higueras thrust as a single structure along this southern section (Fig. 2), but it is quite feasible to link the thrust trace as mapped at the Las Peñas-Las Higueras range with the neotectonic evidences described as the Cerro La Cal fault (Keidel, 1910; Fossa Mancini, 1942; Dessanti, 1942; Bastías et al., 1993; INPRES, 1989; Mingorance, 2000; 2006; Schmidt et al., 2011; Salomon et al., 2013, among others). Accordingly, we integrate here the Cerro La Cal fault trace with the mapped trace of the Las Higueras thrust further north in the Salagasta-La Bomba area (Ahumada, 2004). The reconstructed trace of the southern section exhibits a gentle right bend in plan view and it is possible that more than one fault trace were involved in its surface expression.

4. Holocene activity of the Las Higueras thrust at the Northern section

Evidence of Quaternary activity related to the LHT stand out at the valley of the Montaña river (Fig. 2) (Ahumada, 2010; Ahumada and Costa, 2009). Thrust propagation has here resulted in the development of an east-verging monocline on the oldest remains of terrace deposits, with a 15° front limb slope and average unevenness of 50 m (Fig. 3). The thrust overrides Neogene bedrock over Holocene deposits with an orientation of 170°/25° (right hand rule) and local variations at the submeter scale. A 6 m-high exposure of a partially preserved fold-limb scarp in younger terrace deposits 600 m to the west of the Puesto Santa Clara, accounts for the propagation of this structure during the last 8 ka (Figs. 3, 4 and 5). Stratigraphic markers within Quaternary sediments at the deformed zone along with charcoal-bearing beds, makes this exposure suitable for constraining the Holocene thrust rate.

4.1. Stratigraphy of the deformation zone

Four main sedimentary sequences have been distinguished in the thrust-related stratigraphy, according to their lithology and interpreted evolutionary stages of the thrust propagation (Fig. 5 and Table 2).

Sequence 4 involves alluvial sediments assigned to the Mariño Formation (Miocene) (Sepúlveda and López, 2001), which defines the stratigraphic base for reconstructing the observed Quaternary activity of the LHT. At the deformation zone, these rocks exhibit a shear fabric with prevailing attitudes ranging between 135°/25° and 150°/65°.

Sequence 3 corresponds to the core of the fault-propagated fold. It is predominantly composed by grey-reddish alluvial sands and gravels folded in the hanging wall, whereas they are flat-lying in the footwall. The original attitude of these beds has been transposed by faulting and they were partly eroded after deformation. Therefore, stratigraphic correlation between the hanging wall and footwall mostly relies on lithofacial attributes.

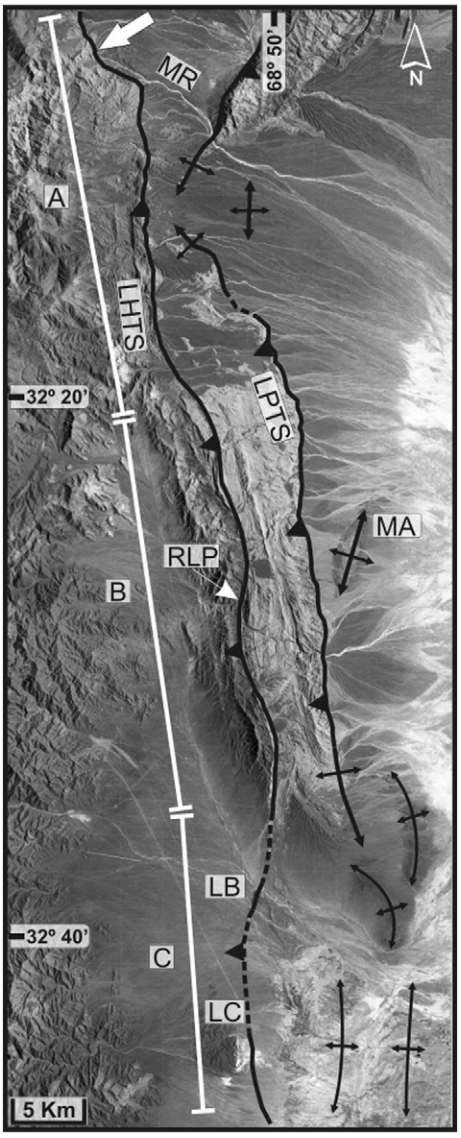

Fig. 2. Landsat TM view of the Andean orogenic front at the Sierra de Las Peñas-Las Higueras showing the location of the Las Higueras (LHT) and the Las Peñas (LPT) thrusts, the Montecito anticline (MA) and the Las Peñas river (RLP). LB, La Bomba hills; LC, La Cal hill; MR, Montaña river. A, B, and C indicate respectively the northern, central and southern sections of the Las Higueras thrust system. The white arrow points out the Puesto Santa Clara zone and the study outcrop shown in Figs. 3, 4 and 5.

Sequence 2 overlies Sequence 3 units in the footwall, being partly unconformable in the hanging wall. The composition of this sequence in the hanging wall corresponds to a mixture of colluvial, wash slope and fluvial sediments. In contrast, typical fluvial beds prevail in the footwall units.

Sequence 1 involves the youngest and least deformed sediments, mostly preserved at the footwall. They correspond to alluvial sediments and a mixture of wash-slope and aeolian deposits at the top. The gentle eastward tilt of its lower unit could be interpreted as a primary slope of local erosive/depositional processes, rather than a consequence of the last propagation stage of the monocline forelimb, because older sequences are less tilted at the footwall (Figs. 4 and 5).

A detailed description of stratigraphic units preserved at the deformation zone is given in Table 2.

4.2. Geometry of the deformation zone

The propagation of the Las Higueras thrust surface during the Holocene resulted in faulting and folding of the hanging wall stratigraphy (Fig. 5A). The thrust is cored by sheared siltstone and sandstone of the Mariño Formation (Sequence 4) and its surface exhibits a flat and ramp geometry with an average dip of 25°W, highlighted by a preferred orientation of planar minerals and closely spaced shear planes.

The lower thrust section has a rather planar surface, dipping 25°W in average, with local variations ranging from 18° to 35°W. It involves the Mariño Formation and east-dipping units of the Sequence 3 at the hanging wall, exhibiting disharmonic meso-miniscopic folds. The main concentration of the shear fabric comprises a 5 to 15 cm thick zone. Gentle or no bed perturbation is observed in the footwall, whereas the massive disposition of most hanging wall units precludes a more detailed analysis of the deformation geometry.

The middle section corresponds to a fault bend, where the thrust-related shear and folding zone flattens over the top of the gravel-rich facies of Unit 22a. Shear effects are here concentrated almost entirely in the gravel-rich facies within a thickness of 3–5 cm.

Sedimentary units within the upper thrust section (S2 and S3) are considered to be deformed by thrust propagation. Overturned beds, according to the brittle shear zone attitude, are clearly visible along this section. The shear zone involves mostly fine-grained sediments of Sequence 2 (Unit 22a).

It has not been possible to properly define the fault tip because this part of the exposure falls into a gully, where variable perspective angles result in different interpretations of the fault geometry (Fig. 5). The tip zone of the propagating thrust might have been eroded and later covered by Sequence 1, although most plausible solutions when modelling

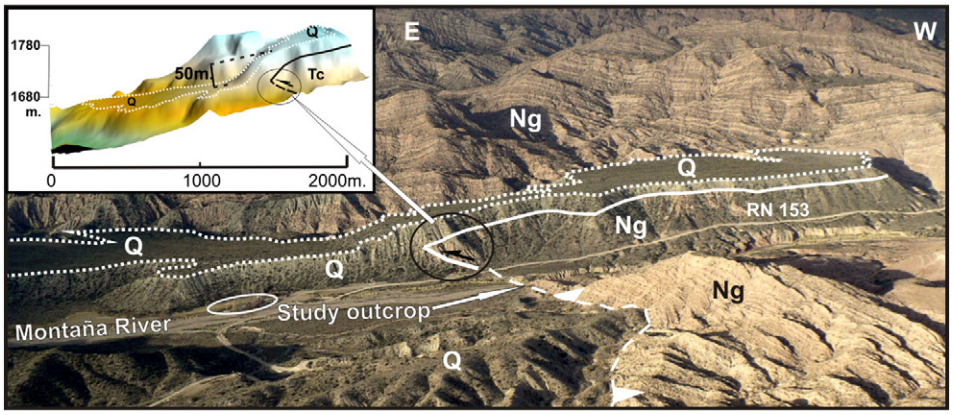

Fig. 3. Oblique aerial view of the Puesto Santa Clara (within white ellipse) area. The LHT trace is shown by white dashed line. Its propagation is highlighted by an east-facing monocline deforming old terrace deposits, whose preserved surface is bounded by dotted lines. Solid line delineates the partly exposed contact between the Neogene (Ng) rocks and the Quaternary (Q) deposits. RN 153, Main road. Inset shows topographic details of the referred monocline obtained through a tripod-LIDAR survey.

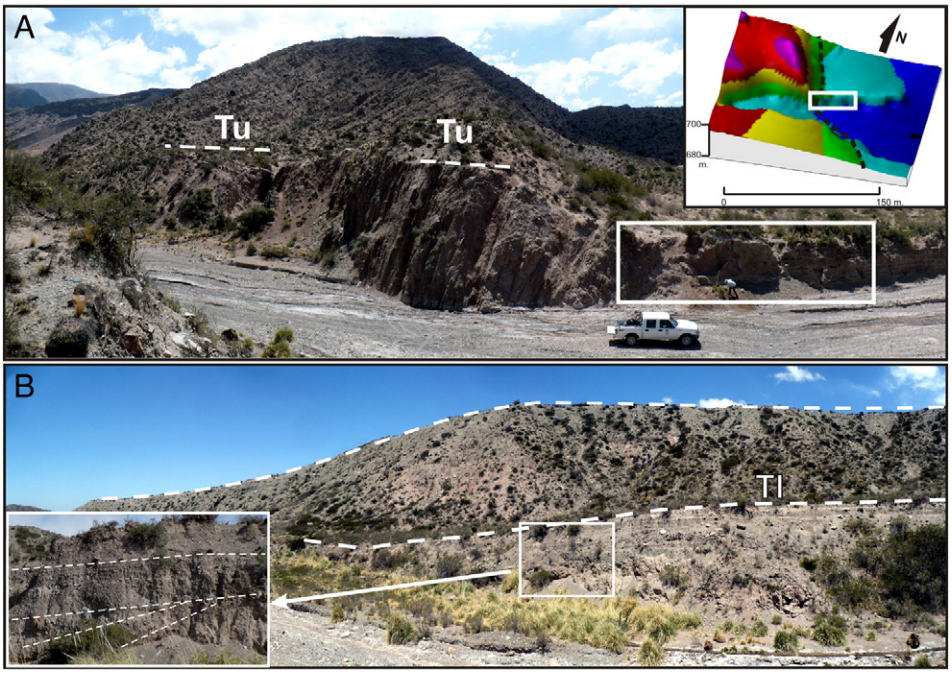

Fig. 4. A. Northwest-looking view of the study outcrop (see geologist for scale). Dashed line highlights the remnants of the upper strath surface (Tu). Inset shows the detailed topography of the study outcrop surveyed through kinematic GPS. B. South looking view of the southern river margin, as seen from the study outcrop. Tl surface points out the gentle flexure in young terrace deposits located in front of the study outcrop. Inset shows growth strata geometry related to the monocline. Main monocline representing larger cumulated deformation of the LHT, as shown in Fig. 3, appears in the background sketched with white dashed line.

the resulting folding geometry suggest the tip line being located nearby the red marker in Sequence 2 (See Chapter 5 and Fig. 6). We are aware that other interpretations are also possible, but a reliable solution as this regards remains uncertain to us with the available field data.

A concentration of shear phenomena in the massive rocks of the Mariño Formation indicates the presence of another fault (F2) in the hanging wall, whose projection into the alluvial cover above coincides with the minor folding described in Sequences 3 and 2 units.

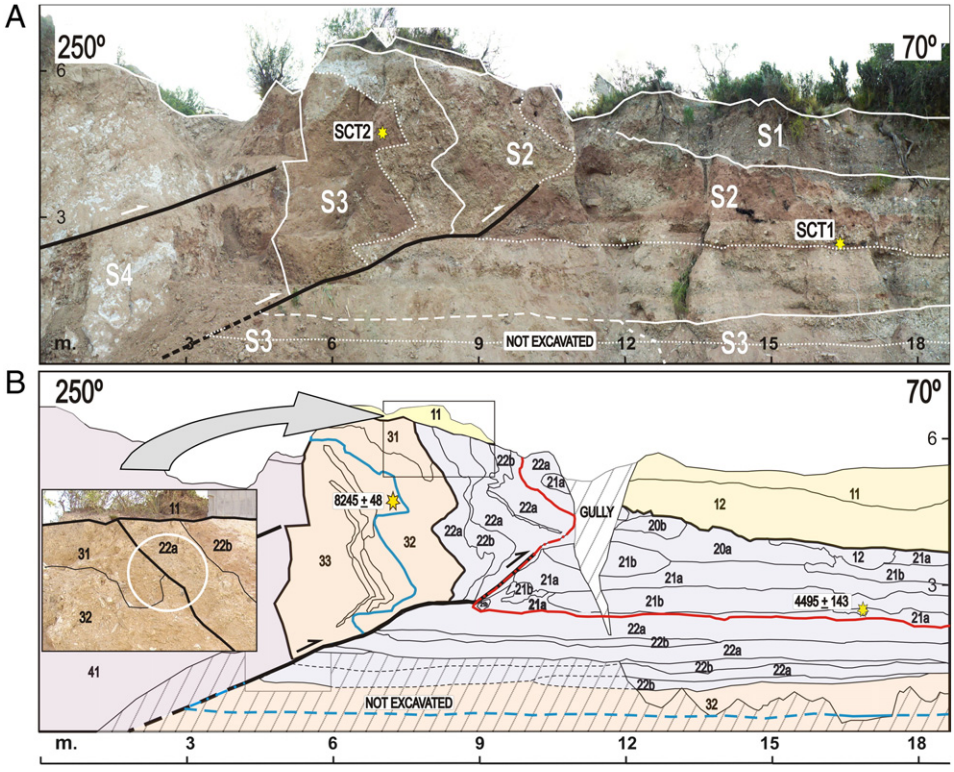

Fig. 5. A. Exposure of the LHT deformation zone at the Montaña river (32°07′05.16″S/68°57′40.68″W), after cleaning and rectification. S1 to S4 refer to the different sedimentary sequences identified. B. Interpretation log of the above referred exposure, showing the disposition of lithologic units (see Table 2 for details). Yellow stars indicate the location of the ^{14}C dated charcoal samples. Fault surface and sedimentary sequences boundaries are shown with thicker lines, although distinguishing sedimentary from tectonic contacts is not simple nearby the thrust propagation zone. Red and blue lines correspond to the restored horizons related to SCT1 and SCT2 samples respectively.

Table 2
Description of the lithostratigraphic units related to the LHT deformation zone at the study site.

Lithostratigraphic units of the deformation zone
Sequence 1
Unit 12: Angular to subangular volcanic and green sandstone gravels in a matrix formed by sandy silt, very pale orange (10 YR 8/2) in color. Poorly sorted and barely stratified, matrix- and clast-supported sediment. Cobble increase in abundance to the top of the unit, with the average size being ~15 cm. It exhibits tabular geometries and well defined contacts at top and base.
Unit 11: Top soil. Massive, light-brownish silty sand.
Sequence 2
Unit 22. Poorly stratified pale grey gravel with rather tabular geometry at the footwall, interbedded with layers of sand and silt. These two dominant lithofacies can be described as follows:
Facies a (22a in Fig. 5). Very pale orange poorly sorted gravel (10 YR 8/2) with a silty sandy matrix. Beds are slightly stratified and exhibit matrix and grain supported fabric, with angular to subangular volcanic and green sandstones clasts. Random cobbles up to 25 cm in diameter are present. The geometry is rather tabular with a sharp base and irregular boundaries at the top. Well-sorted round pebbles prevail near the shear zone.
Facies b (22b in Fig. 5). Sand and silt with sparse gravels. Its fabric is massive to crudely stratified. Prevailing colors are orange pink (10 R 7/4) and grayish orange pink (5 YR 7/2). In the footwall these beds are rather tabular to lens-shaped, contrasting with the dramatic changes in thicknesses in the hanging wall.
Unit 21 is characterized by silty sand, interbedded with gravels. Fine-grained sediments prevail at the footwall. Two main lithofacies can also be here distinguished:
Facies a (21a in Fig. 5). Silty sand with scattered angular gravels orange pink in color (10 R 7/4) massive to crudely stratified. It bears dark-colored organic-rich levels and remains of unclassified bones at its base. *In situ* charcoal pieces within a cross-laminated bed also clearly stand-out at one of these beds. A ^{14}C dating of a sample of detrital charcoal collected from this unit yielded an age of 4495 ± 80 cal years BP (Fig. 5 and Table 3).
Facies b (Unit 21b in Fig. 5). Poorly sorted gravel, matrix and clast-supported with very pale orange color (10 YR 8/2). Angular to subangular volcanic and green sandstone clasts stand out in the sandy-silty matrix. These deposits exhibit a lenticular to tabular bedding shape whose contacts are well defined at the base but usually irregular at the top.
Sequence 3
Unit 33. Silty-gravelly sand, roughly stratified and partly massive, poorly to moderately sorted. Clasts (5–10%) are subangular to subrounded, derived from volcanics and green sandstone. Two discontinuous folded gravel horizons (10–15 cm thick) can be distinguished in the hanging wall. Prevailing colors vary among grayish orange pink (5 YR 7/2), moderate orange pink (10 R 7/4) and very pale orange (10 YR 8/2). These gravel strata highlight a well developed hinge at its base, recording the overturning caused by the propagating thrust. Detrital charcoal collected near the top of this unit (Fig. 5) resulted in a ^{14}C age of 8245 ± 48 cal years BP (Table 3).
Unit 32. Poorly stratified to massive gravel of very pale orange color (10 YR 8/2), matrix (sand and silt) and clast-supported. Clasts are up to 15 cm in diameter, some of which are weathered. The upper boundary of this unit is well defined, exhibiting erosive contacts with Unit 22 and concentration of calcareous paleosoils.
Unit 31. Massive brownish silty sand with sparse gravels. The contact with the lower unit is generally well defined by different composition and a lower concentration of carbonates. The top of Unit 31 has been eroded and is unconformably overlain by Units 22 and 11.
Sequence 4 (*Mariño Formation*, *Miocene*)
Unit 41. Fine to coarse sandstone, interbedded with fine conglomerate and pelitic strata. Grayish to orange pink colors (5 YR 7/2) prevail.

It is not clear how many coseismic slip events are involved in the overall deformation at the study site. However, the local unconformity observed between Sequences 2 and 3 (Fig. 5A) suggests an unsteady prevalence of tectonic, erosive and sedimentation events. Preserved stratigraphy precludes elucidating if such events have produced surface ruptures or if only blind fault-propagation folding prevailed instead.

5. Methods and results

5.1. Ages

The heterogeneous composition of the sedimentary sequences allows distinguishing several layers which highlight the deformation geometry. Radiocarbon data obtained from collected charcoal are located right above (sample SCT1) and nearby (sample SCT2) of two of these key strata, allowing to link the geometry of the deformation with numerical ages (Fig. 5 and Table 3).

Sample SCT1 was collected inside a concentration of detrital charcoal within a thin stratum of very fine gravels in a sandy and silty matrix (Sequence 2). This bed shows small channel geometries, flat tops and irregular bases. It belongs to the undisturbed footwall stratigraphy (Fig. 5) and dating results yielded an age of 4495 ± 143 cal yr BP.

Sample SCT2 corresponds to an isolated piece of detrital charcoal, located in the hanging wall (Unit 33, Sequence 3). Numerical ages resulted in 8245 ± 48 cal yr BP through AMS measurement.

Conventional ages were calibrated through OxCal Radiocarbon Calibration Program v.4.2.4 (Bronk Ramsey, 2009; Bronk Ramsey and Lee, 2013), using the r:5 IntCal 13 atmospheric curve (Reimer et al., 2013) and the ShCal04 calibration curve (McCormac et al., 2004) (Table 3). Calibrated age ranges (4753–4239 cal yr BP for sample SCT1 and 8324–8174 cal yr BP for sample SCT2) were used for estimating rates instead of the mean given ages, in order to better encompass the possible maxima and minima age values for both samples. These ages allow to estimates shortening rates for different time spans at the study site.

5.2. Assumptions and modelling

The upper part of the thrust hanging wall has been eroded for the most part. Therefore some assumptions must be made in order to constrain the possible geometries of the key markers for estimating shortening.

The red marker (Figs. 5, 6, 7 and Table 2) corresponds to a reddish-pink fine-grained bed. This marker was selected because location of sample SCT1 lies directly above it. Photologging and detailed mapping of the exposure (1:100 scale) led us to correlate this bed with the uppermost fold hinge exposed.

The blue marker (Figs. 5, 6, 7 and Table 2) corresponds to a clear lithologic contact defined by the base of the coarse-grained Unit 32 (Sequence 3), which is very proximal (35 cm) to sample SCT2 location. Concentrated brittle shear and distortion of the original strata geometry along the thrust propagation zone, hinders a reliable correlation of strata between both thrust walls. This marker was used for estimating shortening, but due to the uncertainties referred, results are considered to be less reliable than those provided by the red marker.

Our first approach for constraining the possible maximum and minimum lengths of the selected markers at the missing part of the fold, was based on field observations. Remains of an uppermost strath terrace preserved in bedrock at the hanging wall (Tu in Fig. 4A) were surveyed with detailed topographic data (kinematic GPS and tripod-LIDAR). The array of local morphostratigraphic units (Fig. 4) suggests that such erosive remnant predates deposition of Sequences 2 and 3. If so, the altitudinal datum of this surface (Tu) should be at most equal, although most probably higher than the projection in the hanging wall of undeformed flat-lying eroded layers of Sequences 2 and 3. Surface Tu should have accrued a larger vertical displacement than the referred sequences. Therefore, this surface datum constrains the uppermost boundary for both geometric markers in the hanging wall.

On the other hand, well preserved unpaired river terrace deposits extend at both sides of the thrust trace at the southern river margin (Figs. 3 and 4B). These alluvial deposits are nested within the terrace deposits described and exhibit less cumulated deformation than observed in Sequence 2. Thus, they are interpreted to be younger in age than the stratigraphy of the study outcrop. A very gentle monocline imprinted on

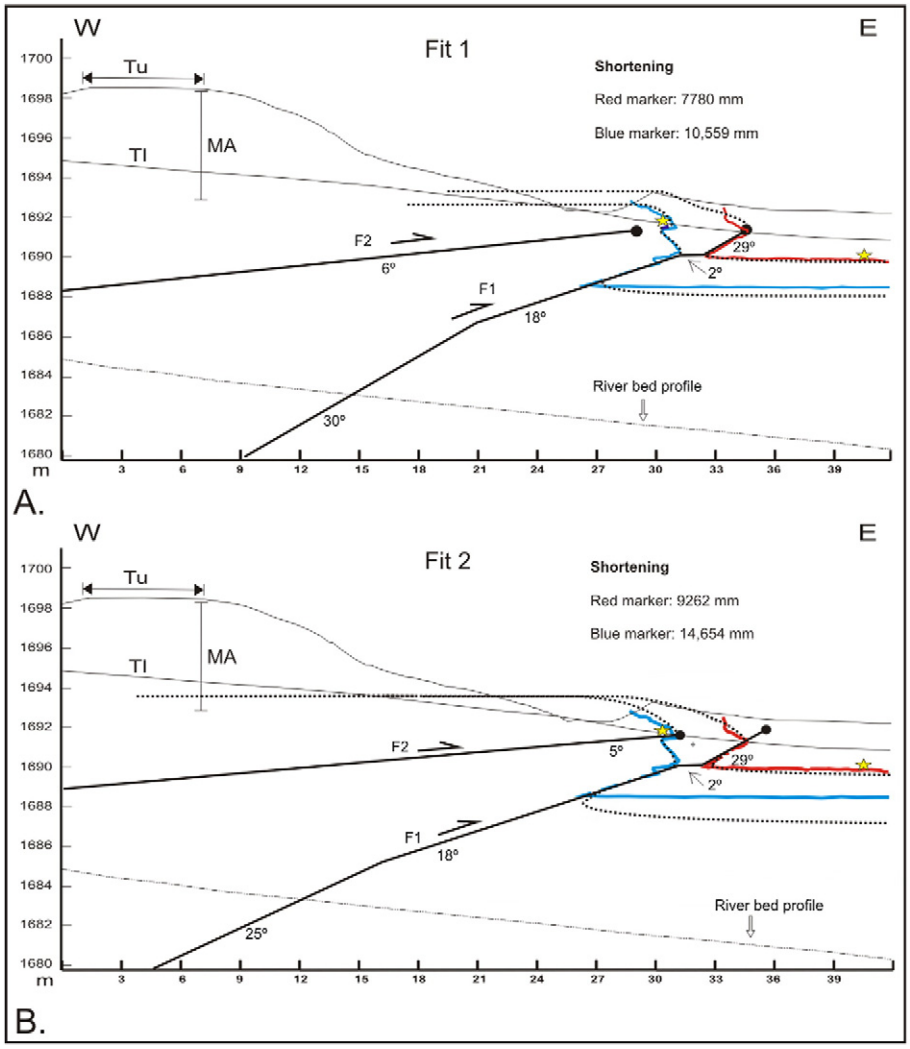

Fig. 6. Selected curves obtained through trishear modelling with the selected best fits for each marker represented with dotted black lines. Solid thin lines represent the outcrop topography, where remains of the uppermost strath terrace (Tu) are indicated and the lowest river terrace surface (Tl). The subtle warping recorded in this alluvial surface is understood to constrain the lowest datum of the maximum possible monocline amplitude (MA). The red and blue lines are related respectively to the layers yielding radiocarbon ages of 4495 ± 143 cal. years BP and 8245 ± 48 cal. years BP. Details on the parameters for modeling these folds are shown in Table 4.

this terrace surface above the projection of the thrust trace (Tl in Figs. 4B, 6 and 7) is understood to be the result of an incipient thrust propagation into sediments younger than Sequence 2. Terrace deposits exhibit dipping angles ranging from 30°E to 14°E in an onlap array at this subtle flexure zone, which are higher than the general terrace slope (6°E) (Fig. 4B). Hence, this fold geometry was considered to be the minimum possible vertical displacement of both markers related to the propagating fold. A topographic cross-section of terrace surface Tl (flipped) showing this gentle folding is depicted with dotted line in Figs. 6 and 7.

The deformation here described cannot be regarded as a parallel type of folding. Significant thickness variation and complexes geometries exposed, as well as incomplete information on the strata geometry at the hanging wall (Fig. 5) precludes the use of the line length and area balance methods (Woodward et al., 1989) to reliably determine shortening. Furthermore, most deposits are consolidated or weakly consolidated at present, but their mechanical condition during Holocene deformation is unknown. Probable changes in density and volume of beds at the deformation zone are likely.

The reconstructed markers show a general up-dip loss of displacement, which along with the folds shape suggest that the exposed deformation can be modeled as a fault propagation fold. The trishear model was used (Allmendinger, 1998; Erslev, 1991; Zehnder and Allmendinger, 2000) to link the observed folding geometry with kinematically balanced sections by means of a forward-modelling procedure. With this purpose, the logged geometries of red and blue markers were displayed in the background of the computer screen (Fig. 6). The parameters controlling the geometry of trishear folding

Table 3
Radiocarbon (^{14}C) dates resulting from charcoal-derived samples STC 1 and STC 2 analyzed at the LATYR (Laboratorio de Tritio y Radiocarbono, La Plata, Argentina) and UCIAMS (UC Irvine AMS Facility) respectively. The latter was measured by AMS technique. Sample preparation backgrounds have been subtracted, based on measurements of ^{14}C-free wood. δ^{13} values for sample STC 2 were measured on prepared graphite using the AMS spectrometer. See text for other details.

Sample name	Lab. ID	$\delta^{13}C$ (‰)	Fraction modern	$\delta^{14}C$ (‰)	^{14}C age (BP)	95.4% (2σ) cal age range (cal yr BP)	^{14}C age cal yr BP (mean)
STC 1	LATYR LP2049	−24 ± 2	0.603 ± 0.0006	−396.9 ± 6.3	4060 ± 80	4815–4239	4495 ± 143
STC 2	UCIAMS 73,820	−20,4 ± 0,1	0.3951 ± 0.0008	604.9 ± 0,8	7460 ± 20	8324–8174	8245 ± 48

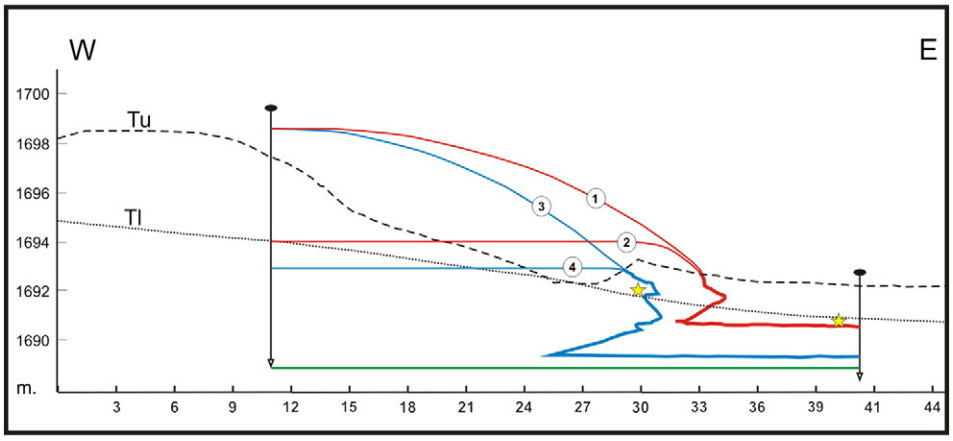

Fig. 7. Maximum (curves 1 and 3) and minimum (curves 2 and 4) shortening estimated for each marker as referred to the green line length, assuming unbalanced fold geometries constrained by the uppermost (Tu) and lowest (Tl) terrace levels. Stars indicate location of samples SCT1 and SCT2 on red and blue markers. See text and Table 5 for details.

(angle of trishear zone, ramp angle, tip point position, P/S ratio) (Table 4) were combined and modified through a trial and error procedure, until finding the better fits.

The local unconformity described between Sequences 2 and 3 (Fig. 5A) points out that perhaps not all of the displacement took place after the deposition of Sequence 2. This observation implies that Sequence 3 should have undergone more cumulated deformation than Sequence 2, not only due to an up-dip loss of displacement of the propagating thrust. We modeled the thrust propagation under different scenarios, either considering Sequence 3 (red marker) being deposited once the deformation of Sequence 2 (blue marker) had already started (growth strata array) or assuming that thrust-related deformation was propagated into the described sediments after the deposition of Sequence 3. Best fitting results were accomplished under the first interpretation (Fig. 6), although in both cases the fold amplitudes are constrained by the upper and lower boundaries (Tu and Tl) suggested by field observations.

Deformation of both markers considered two faults with similar ramp angles, the tip line of the western one (F2 in Fig. 6) lying in the bedrock. Fault F2 is revealed by a concentration of shear phenomena in the Mariño Formation and by minor folding, mainly in Unit 32 (Fig. 5). These modeled curves involve shortening values for the red markers ranging from 7780 mm to 9262 mm (Fig. 6 and Table 5).

Different alternatives in finding the best fits for the blue marker always resulted in flat layers presumably located at the foot wall below the excavated area. Therefore, more reliability is given to the results provided by the red marker. Selected alternatives involved a shortening ranging from 10,559 mm to 14,654 mm (Fig. 6 and Table 5).

5.3. Shortening rate estimation and uncertainties involved

The missing part of the thrust hanging wall constitutes the main source of epistemic uncertainty, being difficult to constrain the range of error involved in the shortening obtained through the trishear model. Fold geometries obtained through computer modelling constitute a simplification of the observed deformation, whose geometric complexities at a centimeter scale could not be suitably reproduced. Therefore, when compared with the markers geometry, the folding shapes obtained through the trishear model, seem to represent a minimum shortening length. Also, the predicted markers geometry at the

Table 4
Parameters involved in the trishear modelling for obtaining shortening lengths and derived shortening rates for each dated horizon. Two curves provided by the software were selected for each marker through graphic comparison with the logged folding to calculate shortening. The amount of shortening corresponding to each marker was related with the maximum and minimum age results for each layer, in order to obtain the minimum and maximum estimated shortening rates. Trishear modelling was done using the FaultFoldForward v.6.2.0 software developed by R. Allmendinger (http://www.geo.cornell.edu/geology/faculty/RWA/programs/faultfoldforward.html; last accessed May 2015).

Model	Trishear parameters					Shortening (mm)
	Ramp angle	Apical angle (trishear zone)	Propagation slip Ratio (P/S)	Partial slip (m)	Trishear field velocity	
Fit 1	Fault 1 (Multi-bend Fault)					Red marker: 7780 Blue marker: 10,559
	30°	30°	2.2	.12*	Linear	
	30°	30°	29°	3.03	Linear	
	18°	30°	29°	4.76	Center concentrated	
	2°	30°	29°	0.48	Center concentrated	
	29°	30°	29°	1.06	Center concentrated	
	Fault 2					
	6°	10°	2	1.1	Center concentrated	
Fit 2	Fault 1 (Multi-bend Fault)					Red marker: 9262 Blue marker: 14,654
	25°	35°	2.4	4.61*	Sine	
	25°	35°	2.4	3.49	Sine	
	18°	35°	2.4	6.29	Concentrated sine center	
	2°	35°	2.4	0.47	Concentrated center	
	29	35°	2.4	1.22	Concentrated center	
	Fault 2					
	5°	30°	2.4	1.1	Center concentrated	

Table 5
Parameters used for determining shortening rates. Maximum shortening and minimum ages were used for estimating maximum shortening rates, whereas minimum rates resulted from minimum shortening and maximum ages. Shortening obtained through trishear modelling was preferred for estimating the mean slip and uplift rates.

		Parameter	Red marker	Blue marker
Shortening (mm)	Trishear	Minimum shortening	7780	10,559
		Maximum shortening	9262	14,654
	Unbalanced	Minimum. shortening	5970	14,400
		Maximum shortening	6900	15,480
Ages (Calendar yr BP)		Minimum age	4239	8174
		Maximum age	4815	8324
Rates (mm/a)	Trishear	Minimum shortening rate	1.615	1.268
		Maximum shortening rate	2.184	1.793
	Unbalanced	Minimum shortening rate	1.239	1.729
		Maximum shortening rate	1.627	1.893
	Mean rates	Mean shortening rate (Trishear)	1.90 ± 0.28	1.53 ± 0.26
		Mean shortening rate (unbalanced)	1.43 ± 0.19	1.81 ± 0.08
		Mean slip rate (Trishear)	2.55 ± 0.38	2.02 ± 0.31
		Mean uplift rate (Trishear)	1.07 ± 0.31	0.84 ± 0.24

hanging wall flattens at a similar height than the Tl surface, which is understood to constrain the minimum amplitude of the thrust-related monocline (Fig. 6). Hence, it is thought that estimations here provided for each marker regarding shortening lengths and rates should be considered as conservative or minima values.

The maximum and minimum possible shortening is difficult to address with the available data. However, the relevance of rate estimation encompassing the millennial timescale warrants an attempt to approach relevant errors, even if large. Accordingly, unbalanced fold geometries were also reconstructed as an alternative approach to encompass the maximum and minimum possible fold amplitude for the selected layers. Each marker horizon was divided into two interpretative lines at the hanging wall (Fig. 7) and pin-pointed at the interpreted lowest (lines 1 and 3) and highest possible topographic datum (lines 2 and 4) of surfaces Tu and Tl respectively. In spite of missing data for suitably imaging the hanging wall geometry, it is understood that this approach could help to cross-check field observations with the results provided by balanced cross-sections for constraining the shortening accrued. Shortening values obtained are shown in Table 5. They exhibit no significant variations with shortening values suggested by balanced models and may help to understand the minimum possible rate values for the red marker and the maximum ones for the blue marker.

Regrettably, the surveyed data hinders so far a better refinement of the error involved.

The maximum and minimum shortening rate value for each marker was calculated through a crossed relation between the maximum shortening against the minimum age and vice versa, in order to cover the widest variation range. The values used for estimating the range of shortening rate values through the trishear model and unbalanced cross sections are displayed in Table 5. Shortening rates estimated for the red marker range vary from 1.61 mm/a to 2.18 mm/a for the last 4495 ± 143 ka and slightly lower rates from 1.27 mm/a to 1.79 mm/a for the last 8245 ± 48 ka (blue marker).

The azimuth of the analyzed exposure (70°) is almost perpendicular to the thrust surface. The dominant strike at this outcrop is 170°, with local variations up to 155°. No evidence (i.e. slickenlines, offset surfaces) were found for understanding the possible contribution of the strike-slip component to the total slip vector. In order to properly determine the total slip rate for this structure, the strike-slip component should be estimated in 3D, despite that the thrust trace is quite orthogonal to the regional shortening axis (Kendrick et al., 1999, 2003, 2006).

6. Discussion

Several previous contributions have calculated Neogene shortening rates varying between 4.7 mm/a and 9.5 mm/a at a geological time scale (Table 1). They were derived by estimating the cumulated shortening across different morphostructural units of the Andean orogen at the Southern Pampean flat-slab, although without focusing on the dynamic evolution of individual structures. In this regard, some structures may have become inactive during such a time span (2×10^7–10^6 y) (Meigs et al., 2006), and others may have increased their activity during a much shorter time period. The results presented here correspond to shortening rates for a single structure during a millennial time scale, which implies a different time window as for those contributions addressing decadal and geological time scales (Table 1).

The here estimated rates for the northern LHT correspond to about 18% to 43% of the most likely long-term shortening rates (5–7 mm/a) estimated for the complete width of the Precordillera and the Andean front region of 30–33°S (Table 1). They reasonably fit into the shortening rates suggested by long-term calculations for the whole frontal deformation zone, assuming that total shortening at the entire Andean or Precordilleran orogen scale has been accommodated by several structures and processes over larger temporal scales (see Allmendinger et al., 1990 and other references in Table 1).

Sarewitz (1988) postulated that shortening rates in a foothill structure at the Andean thrust front farther south (La Pilona anticline at 33°S, Table 1, Fig. 1), have exceeded 6 mm/a during the last 2.7 Ma and probably exceeded 16 mm/a during the last 1.0 Ma. This author suggested accordingly that motion on individual thrusts near the orogenic front may occur five to ten times faster than rates averaged over the entire history of the thrust belt, such as in the Rocky Mountains. The referred contribution also postulated that long-term averages ($>10^7$ years) cannot discriminate between dominant tectonic activity and tectonic quiescence, with the thrust front best characterized by pulses of high activity separated by long periods of quiescence. Nonetheless, the rates estimated by Sarewitz (1988) appear to be very high in comparison with those discussed above. The fact that the La Pilona anticline has not developed any significant landscape imprint in the piedmont during the last 2.7 Ma, does not favor to interpret it as a structure with a sustainable high shortening/uplift rate (>6 mm/a).

Confronting the rates here estimated with previous results obtained in analogous time windows (~100 ka), they are similar to the 0.9 ± 0.3–1.5 ± 0.3 mm/a range of shortening rates obtained by Schmidt et al. (2011) for the 12.1 ± 2.4 and 3.9 ± 0.1 ka time interval at the La Cal fault (LHT southernmost exposure, Fig. 2). Our results also fall in the same range of shortening rates (~1.2–2.0 mm/a) postulated for the Holocene shortening in a young splay of the Las Peñas thrust by Schmidt et al. (2011) and for other nearby structures during the Late Pleistocene–Holocene (Bohon et al., 2008; Cisneros et al., 2010; Olgiati and Ramos, 2003; Schoenbohm et al., 2013).

Late Pleistocene slip rates reported for the Villicum-Las Tapias and the La Laja faults in Eastern Precordillera (Fig. 1) are lower (<1 mm/a) than the rates estimated here (Ragona, 2007; Rockwell et al., 2014;

Siame et al., 2002). However, they are consistent with the interpretation of the former structure exhibiting low activity during the Late Pleistocene (Meigs et al., 2006; Vergés et al., 2007) and with the La Laja fault being a secondary thrust-related structure (Ragona, 2007; Rockwell et al., 2014).On a very different timescale, Kendrick et al. (1999, 2001, 2003, 2006) concluded that GPS data indicate similar displacement vectors ranging between 2 mm/a and 4 mm/a at the latitude of this study area of the Andean front, whereas Brooks et al. (2003) estimated 4.5 ± 1.7 mm/a (Table 1). The shortening rates here estimated could represent from 32% to 100% of the ongoing shortening at this latitude, at a decadal time scale (Table 1). Even if our results depict a different time window and deformation processes than those imaged by tectonic geodesy, some implications may arise from this situation:

1 The Holocene and current shortening at these latitudes is being accommodated through few faults and mainly concentrated at the LHT, as also suggested by Schmidt et al. (2011) farther south.
2 There are no other shortening rates so far available, to compare with at this section of the LHT. However, assuming a Late Pleistocene age (<120 ka) for the old terrace deformed by the LHT, 300 m southeast of the study outcrop (Fig. 3), some comments regarding rates variability over time could preliminary be done. These terrace deposits exhibit 50 m of vertical displacement due to the cumulated thrust slip. Averaging the LHT surface in 35°W (Ahumada, 2010), it yields to a shortening rate of ~0.6 mm/a over that time scale. Hence, it might be possible that slip on the LHT has accelerated at least during the Holocene. Higher shortening rates yielded by younger beds at Sequence 2 (4495 ± 143 ka) may also favor this hypothesis, although more data are needed as this regards.
3 Shortening rates obtained, particularly for the last ~4 ka, may overestimate the LHT Holocene slip, at least in comparison with GPS displacement vectors recorded during the last two decades. However, more data are needed to understand relationships between elastic deformation recorded by tectonic geodesy and permanent deformation as expressed here by folded strata.
4 The recurrence interval as for seismic events with related surface deformation at this section of the LHT is unknown as well as the last event with related surface deformation. The timing of latest surface deformation could be bracketed between the age of the undeformed layers of Sequence 1 and the age of the gently folded surface of the terrace deposits located at the southern river margin, but both ages are so far unknown. A surface deformation event (<4 ka) or a cluster of them might yield to overestimate the mean shortening rate, and may hampers to properly asses its temporal variability. This situation probably have biased the interpretation done by Schmidt et al. (2011) and Salomon et al. (2013), who proposed rates almost five times larger for the La Cal fault structure (5.2 ± 1.5 mm/a) during the last 0.8 ka. A time span encompassing at least four or five seismic cycles would be much better suited to understand the possible shortening rate variability over time.

7. Conclusions

Despite some uncertainties posed by the surveyed data, our results place constraints on the shortening rates of the LHT during the last ~ 8 ka at its northern section. Preferred shortening rates obtained by means of kinematically balanced fold geometries for the study site range from 1.90 ± 0.28 mm/a for the last 4495 ± 143 ka to 1.53 ± 0.26 for the last 8245 ± 48 ka. However, they may represent minima rate values, because shortening geometries obtained through are close to the topographic datum related to terrace surface Tl (Fig. 6). This datum is understood to limit the minimum possible amplitude of the thrust related monocline.

According to the shortening rates here reported, Holocene mean dip slip rates for this section of the LHT thrust may range from 1.71 mm/a to 2.93 mm/a and uplift rates vary from 0.60 mm/a to 1.38 mm/a during the last ~8 ka. These estimations result from considering an average thrust dip angle of 25° W at the study outcrop below the interpreted tip line (Table 5 and Fig. 5).

The information provided by this contribution, as well as data presented by Schmidt et al. (2011) at the southern section of the LHT, suggest that most recent activity at this thrust is being concentrated at both ends of its outcropping length.

Acknowledgements

Insightful reviews by R. Allmendinger and S. Mechernich helped to improve a previous version of the manuscript, also benefitted with comments by T. Rockwell, L. Owen and L. Schoenbohm. We are also indebted to the comments and suggestions provided by two anonymous reviewers and the editor through thoughtful and thorough reviews. Tripod-LIDAR topographic data were kindly provided by B. Brooks and T. Ericksen, whereas E. Cristallini assisted with the trishear modelling. Financial support was provided by the Universidad Nacional de San Luis Project CyT 340303.

References

Ahumada, E., 2004. Geología y estructura del extremo sur de la Sierra de Las Peñas, provincia de Mendoza (BSc Thesis) Depto. Geología, Univ. Nac. de San Luis.
Ahumada, E., 2010. Neotectónica del frente orogénico andino entre los 32°08′S–32°19′S, provincias de Mendoza y San Juan (PhD Thesis) Depto. Geología, Univ. Nac. San Luis.
Ahumada, E., Costa, C., 2009. Antithetic linkage between oblique Quaternary thrusts at the Andean front, Argentine Precordillera. J. S. Am. Earth Sci. 28, 207–216. http://dx.doi.org/10.1016/j.jsames.2009.03.008.
Ahumada, E., Costa, C., Gardini, C., Diederix, H., 2006. La estructura del extremo sur de la Sierra de Las Peñas-Las Higueras, Precordillera de Mendoza. Asoc. Geol. Arg, Pub. Esp. 6, 11–17.
Allmendinger, R., 1998. Inverse and forward numerical modeling of trishear fault propagation folds. Tectonics 17 (4), 640–656.
Allmendinger, R., Figueroa, D., Snyder, D., Beer, J., Mpodozis, C., Isacks, B., 1990. Foreland shortening and crustal balancing in the Andes at 30°S Latitude. Tectonics 9 (4), 789–809.
Alvarado, P., Beck, S., Zandt, G., 2007. Crustal structure of the south-central Andes Cordillera and Backarc region from regional waveform modeling. Geophys. J. Int. Tectonics Geodynamics 170 (2), 858–875. http://dx.doi.org/10.1111/j.1365-246X.2007.03452.x.
Bastías, H., Weidmann, N., Pérez, M., 1984. Dos zonas de fallamiento Plio-Cuaternario en la Precordillera de San Juan, presented at the 9th Congreso Geológico Argentino. 2, 329–341.
Bastías, H., Tello, G., Perucca, L., Paredes, J., 1993. Peligro sísmico y neotectónica. 13rd Congreso Geológico Argentino. Relatorio, 645–658. Buenos Aires.
Bea, S., 2000. Geología y estructura de la sierra de Las Peñas, al norte del río homónimo (32°30′ S) Precordillera, provincia de Mendoza, Argentina (BSc Thesis) Dep. de Geología, Univ. Nac. de San Luis.
Bohon, W., Schoenbohm, L., Brooks, B., Costa, C., 2008. Accelerating uplift rate and non-uniform inheritance: cosmogenic Be^{10} depth profiles from the Montecito anticline, Mendoza, Argentina. Eos Trans. AGU 89 (53), T23E-04 (Fall Meet. Suppl. Abstract).
Bronk Ramsey, C., 2009. Bayesian analysis of radiocarbon dates. Radiocarbon 51 (1), 337–360.
Bronk Ramsey, C., Lee, S., 2013. Recent and planned developments of the program OxCal. Radiocarbon 55 (2–3), 720–730.
Brooks, B., Bevis, M., Smalley Jr., R., Kendrick, E., Manceda, R., Lauría, E., Maturana, R., Araujo, M., 2003. Crustal motion in the Southern Andes (26°–36°S): Do the Andes behave like a microplate? Geochem. Geophys. Geosyst. 4 (10). http://dx.doi.org/10.1029/2003GC000505.
Cisneros, H., Costa, C., Gardini, C., 2010. Análisis neotectónico del área Cerro Salinas, Departamento Sarmiento, pcia. de San Juan. Rev. Asoc. Geol. Argent. 67 (4), 439–449.
Cortés, J., Costa, C., 1996. Tectónica Cuaternaria en la desembocadura del Río de las Peñas, Borde oriental de la Precordillera de Mendoza, presented at the 13rd Congreso Geológico Argentino. 2 pp. 225–238.
Cortés, J., Vinciguerra, P., Yamín, M., Pasini, M., 1999. Tectónica Cuaternaria en la región andina del nuevo Cuyo. In: Caminos, R. (Ed.), Geología Argentina 29. SEGEMAR Anales, pp. 760–778.
Cortés, J., Yamín, M., Pasini, M., 2005. La Precordillera Sur, provincias de Mendoza y San Juan, presented at the 16th Congreso Geológico Argentino. 1 pp. 395–402.
Cortés, J., Terrizzano, C., Pasini, M., Yamin, M., Casa, A., 2014. Quaternary tectonics along oblique deformation zones in the Central Andean retrowedge between 31°30′ S and 35°S. In: Sepúlveda, S., Giambiagi, L., Moreiras, S., Pinto, L., Tunik, M., Hoke, G., Farías, M. (Eds.), Geodynamic processes in the Andes of Central Chile and Argentina. Geol. Soc. Special Publ. 399. http://dx.doi.org/10.1144/SP399.5.
Costa, C., Rockwell, T., Paredes, J., Gardini, C., 1999. Quaternary deformation and seismic hazard at the Andean Orogenic Front (31°–33°, Argentina): A paleoseismological perspective, presented at the 4th International Symposium on Andean Geodynamics. pp. 187–191 (Extended Abstracts,).
Costa, C., Diederix, H., Gardini, C., Cortés, J., 2000a. The Andean orogenic front at Sierra de Las Peñas-Las Higueras, Mendoza, Argentina. J. S. Am. Earth Sci. 13, 287–292.

Costa, C., Gardini, C., Diederix, H., 2000b. The Montecito anticline: A Quaternary growing structure in the Precordilleran foothills of northern Mendoza. *Argentina*, presented at the 9th Congreso Geológico Chileno. 1 pp. 758–762.
Costa, C., Gardini, C., Diederix, H., 2005. Tectónica vs. sedimentación en el Río de Las Peñas, Precordillera de Mendoza, presented at the 16th Congreso Geológico Argentino, La Plata.
Costa, C., Audemard, F., Becerra, F., Lavenu, A., Machette, M., París, G., 2006a. An overview of the main Quaternary deformation of South America. Rev. Asoc. Geol. Argent. 61 (4), 461–479.
Costa, C., Gardini, C., Diederix, H., Cisneros, H., Ahumada, E., 2006b. The active Andean orogenic front at the Souhternmost Pampean flat-slab, presented at the Backbone of the Americas. Abstract with programs 15-1.
Costa, C., Ahumada, E., Gardini, C., Vazquez, F., Diederix, H., 2014. Quaternary shortening at the orogenic front of the Central Andes of Argentina (32°15′–32°40′S): A field survey of the Las Peñas thrust. In: Sepúlveda, S., Giambiagi, L., Moreiras, S., Pinto, L., Tunik, M., Hoke, G., Farías, M. (Eds.), Geodynamic processes in the Andes of Central Chile and Argentina. Geol. Soc. Special Publ. 399. http://dx.doi.org/10.1144/SP399.5.
Cristallini, E., Ramos, V., 1997. Estructura profunda de los Andes a los 32° de latitud sur (Argentina y Chile), presented at the 8th Congreso Geológico Chileno, Actas. 3, 1622–1625.
Dellapé, D., Hegedus, A., 1995. Structural inversion and oil occurrence in the Cuyo basin of Argentina. In: Tankard, A., Suárez Soruco, R., Welsink, H. (Eds.), Petroleum basins of South America 62. American Association of Petroleum Geologist Memoir, pp. 369–382.
Dessanti, R., 1942. Geología de la zona del Cerro La Cal, Río de Las Peñas y El Borbollón. YPF, Unpublished report, 39 p.
Erslev, E.A., 1991. Trishear fault-propagation folding. Geology 19, 617–620.
Figueroa, D., Ferraris, O., 1989. Estructura del margen oriental de la Precordillera Mendocina-Sanjuanina, presented at the 1st Congreso Nacional de Exploración de Hidrocarburos. 1 pp. 515–529.
Fossa Mancini, E., 1942. Algunas particularidades del sinclinal de Salagasta, Mendoza. Notas del Museo de la Plata. 7 (18), 39–68.
Giambiagi, L., Ramos, V., 2002. Structural evolution of the Andes in a transitional zone between flat and normal subduction (33°30′–33°45′S), Argentina and Chile. J. S. Am. Earth Sci. 15 (1), 101–116.
Harrington, H., 1971. Descripción geológica de la Hoja 22c, "Ramblón", provincias de Mendoza y San Juan. Dirección Nacional de Geología y Minería, Buenos Airesp. 81 (Boletín 114).
Hindle, D., Kley, J., Stein, S., Dixon, T., Norabuena, E., 2002. Consistency of geologic and geodetic displacements during Andean orogenesis. Geoph. Res. Let. 29 (8), 1–4. http://dx.doi.org/10.1029/2001GL013757.
INPRES, 1989. Microzonificación sísmica del Gran Mendoza, Argentina. Executive Summary 2. Instituto Nacional de Prevención Sísmica, San Juan, p. 121.
Jordan, T., Isacks, B., Allmendinger, R., Brewer, J., Ramos, V., Ando, C., 1983. Andean tectonics related to geometry of subducted Nazca plate. Geol. Soc. Am. Bull. 94, 341–361.
Jordan, T., Allmendinger, R., Damanti, J., Drake, R., 1993. Chronology of motion in a complete thrust belt – the Precordillera, 30–31°S, Andes mountains. J. Geol. 101, 135–156.
Keidel, J., 1910. Informe sobre los trabajos efectuados por la Sección Geología de la División de Minas, Geología e Hidrología en los años 1906, 1907 y 1908. Anales del Ministerio de Agricultura, Sección Geología, Mineralogía y Minas, Buenos Aires 5. 2, pp. 26–77.
Kendrick, E., Bevis, M., Smalley Jr., R., Cifuentes, O., Galbán, F., 1999. Current rates of convergence across the Central Andes; estimates from continuous GPS observations. Geophys. Res. Lett. 26, 541–544.
Kendrick, E., Bevis, M., Smalley Jr., R., Brooks, B., 2001. An integrated crustal velocity field for the central Andes. Geochem. Geophys. Geosyst. 2, 11. http://dx.doi.org/10.1029/2001GC000191.
Kendrick, E., Bevis, M., Smalley Jr., R., Brooks, B., Vargas, R., Lauría, E., Fortes, L., 2003. The Nazca-south America Euler vector and its rate of change. J. S. Am. Earth Sci. 16, 125–131.
Kendrick, E., Brooks, B., Bevis, M., Smalley Jr., R., Lauria, E., Araujo, M., Parra, H., 2006. Active orogeny of the South-Central Andes studied with GPS geodesy. Rev. Asoc. Geol. Argent. 61 (4), 555–566.
McCormac, F., Hogg, G., Blackwell, P., Buck, C., Higham, T., Reimer, P., 2004. SHCal04 southern hemisphere calibration, 0–11.0 cal kyr BP. Radiocarbon 46 (3), 1087–1092.
Meigs, A., Nabelek, J., 2010. Crustal scale pure shear foreland deformation of Western Argentina. Geophys. Res. Lett. 37, L11304. http://dx.doi.org/10.1029/2010GL043220.
Meigs, A., Krugh, W., Schiffman, C., Vergés, J., Ramos, V., 2006. Refolding of thin-skinned thrust sheets by active basement-involved thrust faults in the eastern Precordillera of western Argentina. Rev. Asoc. Geol. Argent. 61 (4), 589–603.
Mingorance, F., 2000. Caracterización de la geometría de la zona de fallamiento activo La Cal, Mendoza - Argentina, presented at the 9th Congreso Geológico Chileno, 1, 800–804.
Mingorance, F., 2006. Morfometría de la escarpa de falla histórica identificada al norte del Cerro La Cal, zona de falla La Cal Mendoza. Rev. Asoc. Geol. Argent. 61 (4), 620–638.
Olgiati, S., Ramos, V., 2003. Neotectónica Cuarternaria en el Anticlinal Borbollón, Provincia de Mendoza - Argentina, presented at the 10th Congreso Geológico Chileno (11 pp.).
Ortiz, A., Zambrano, J., 1981. La provincia geológica Precordillera Oriental, presented at the 8th Congreso Geológico Argentino. 3 pp. 59–74.
Perucca, L., Paredes, J., 2002. Peligro sísmico en el departamento Albardón y su relación con el área de fallamiento La Laja, provincia de San Juan. Rev. Asoc. Geol. Argent. 57 (1), 45–54.
Perucca, L., Ruiz, F., 2014. New data on neotectonic contractional structures in Precordillera, south of Río de La Flecha: Structural setting from gravity and magnetic data. San Juan, Argentina. J. S. Am. Earth Sci. 50, 1–11.
Perucca, L., Vargas, N., 2014. Neotectónica de la provincia de San Juan, centro-oeste de Argentina. Bol. Soc. Geol. Mex. 66 (2), 291–304.
Ragona, D., 2007. Advanced methods and techniques in paleoseismology (PhD Thesis) Dep. of Geol., University of California San Diego.
Ramos, V., 1988. The tectonics of the Central Andes; 30° to 33°S latitude. In: Clark, S., Burchfiel, C. (Eds.), Processes in continental lithospheric deformationGeological Society of America Special Paper 218. Boulder, CO, pp. 31–54.
Ramos, V., Kay, S., 1991. Triassic rifting and associated basalts in the Cuyo basin, central Argentina. In: Harmon, R., Rapela, C. (Eds.), Andean magmatism and its tectonic settingGeological Society of America Special Paper 265. Boulder, CO, pp. 79–91.
Ramos, V., Cegarra, M., Cristallini, E., 1996. Cenozoic tectonics of the High Andes of West-Central Argentina (30–36°S latitude). Tectonophysics 259, 185–200.
Ramos, V., Cristallini, E., Pérez, D., 2002. The Pampean flat-slab of the Central Andes. J. S. Am. Earth Sci. 15, 59–78.
Ramos, V., Zapata, T., Cristallini, E., Introcaso, A., 2004. The Andean thrust system-Latitudinal variations in structural styles and orogenic shortening. Am. Assoc. Petr. Geol. Mem. 82, 30–50.
Reimer, P., 29 others, 2013. IntCal 13 and Marine 13 radiocarbon age calibration curves 0–50,000 years Cal BP. Radiocarbon 55 (4), 1869–1887.
Rockwell, T., Ragona, D., Meigs, A., Owen, L., Costa, C., Ahumada, E., 2014. Inferring a thrust-related earthquake history from secondary faulting: A long rupture record of La Laja Fault, San Juan, Argentina. Bull. Seismol. Soc. Am. 104 (1), 269–284. http://dx.doi.org/10.1785/0120110080.
Salomon, E., Schmidt, S., Hetzel, R., Mingorance, F., Hampel, A., 2013. Repeated folding during late Holocene earthquakes on the La Cal thrust fault near Mendoza city (Argentina). Bull. Seismol. Soc. Am. 103 (2), 936–949. http://dx.doi.org/10.1785/0120110335.
Sarewitz, D., 1988. High rates of late Cenozoic crustal shortening in the Andean foreland, Mendoza Province, Argentina. Geology 16, 1138–1142.
Schmidt, S., Hetzel, R., Mingorance, F., Ramos, V., 2011. Coseismic displacements and Holocene slip rates for two active thrust faults at the mountain front of the Andean Precordillera (~33°S). Tectonics 30, TC5011. http://dx.doi.org/10.1029/2011TC002932.
Schmidt, S., Tsukamoto, S., Salomon, E., Frechen, M., Hetzel, R., 2012. Optical dating of alluvial deposits at the orogenic front of the Andean Precordillera (Mendoza, Argentina). Geochronometria 39, 62–75. http://dx.doi.org/10.2478/s13386-011-0050-5.
Schoenbohm, L., Costa, C., Brooks, B., Bohon, W., Gardini, C., Cisneros, H., 2013. Fault interaction along the Central Andean thrust front: The Las Peñas thrust, Cerro Salinas thrust and the Montecito anticline. Eos Transactions Am. Geoph. Union. 94 (Fall Meet. Suppl., Abstract T31D-2543.).
Sepúlveda, E., López, H., 2001. Descripción geológica de la Hoja 3369-II Mendoza, provincia de Mendoza. SEGEMAR, Boletín 252, Buenos Aires.
Siame, L., Bellier, O., Sébrier, M., Bourlès, D., Leturmy, P., Perez, M., Araujo, M., 2002. Seismic hazard reappraisal from combined structural geology, geomorphology and cosmic ray exposure dating analyses: the Eastern Precordillera thrust system (NW Argentina). Geophys. J. Int. 150 (1), 241–260. http://dx.doi.org/10.1046/j.1365-246X.2002.01701.x.
Siame, L., Bellier, O., Sébrier, M., Araujo, M., 2005. Deformation partitioning in flat subduction setting: Case of the Andean foreland of western Argentina (28°S–33°S). Tectonics 24 (5), TC5003. http://dx.doi.org/10.1029/2005tc001787.
Siame, L., Bellier, O., Sebrier, M., 2006. Active tectonics in the Argentine Precordillera and Western Sierras Pampeanas. Rev. Asoc. Geol. Argent. 61 (4), 604–619.
Smalley Jr., R., Isacks, B., 1987. A high resolution local network study of the Nazca Plate Wadati-Benioff zone under western Argentina. J. Geophys. Res. 92, 13.093–13.912.
Smalley Jr., R., Isacks, B., 1990. Seismotectonics of Thin- and Thick- Skinned Deformation in the Andean Foreland from local Network Data: Evidence for a seismogenic Lower Crust. J. Geophys. Res. 95, 12,487–12,498.
Smalley Jr., R., Pujol, J., Regnier, M., Chiu, J.M., Chatelain, J., Isacks, B., Araujo, M., Puebla, N., 1993. Basement seismicity beneath the Andean Precordillera thin-skinned thrust belt and implications for crustal and lithospheric behavior. Tectonics 12, 63–76.
Vergés, J., Ramos, V., Meigs, A., Cristallini, E., Bettini, F., Cortés, J., 2007. Crustal wedging triggering recent deformation in the Andean Thrust front between 31°S and 33°S: Sierras Pampeanas-Precordillera interaction. J. Geophys. Res. 112, B03 S15. http://dx.doi.org/10.1029/2006JB004287.
Wichmann, R., 1928. Datos geológicos sobre la región de Salagasta, Mendoza. Ministerio de Agricultura de la Nación. Dirección General de Minas, Geología e Hidrología. Publicación N° 37, Buenos Aires.
Woodward, N., Boyer, S., Suppe, J., 1989. Balanced geological cross-sections: an essential technique in geological research and exploration. presented at 28th International Geological Congress, Washington, DC (pp. 132).
Zapata, T., Allmendinger, R., 1996. Thrust front zone of the Precordillera, Argentina: a thick-skinned triangle zone. Bull. Am. Assoc. Petrol. Geol. 80, 359–381.
Zehnder, A., Allmendinger, R., 2000. Velocity field for the trishear model. J. Struct. Geol. 22, 1009–1014.